Solid-State NMR Spectroscopy of Membrane-Associated Myelin Basic Protein—Conformation and Dynamics of an Immunodominant Epitope

Mumdooh A. M. Ahmed,[†§] Vladimir V. Bamm,[‡§] George Harauz,[‡§*] and Vladimir Ladizhansky[†§*]
[†]Department of Physics and [‡]Department of Molecular and Cellular Biology, and [§]Biophysics Interdepartmental Group, University of Guelph, Guelph, Ontario, Canada

ABSTRACT Myelin basic protein (MBP) maintains the tight multilamellar compaction of the myelin sheath in the central nervous system through peripheral binding of adjacent lipid bilayers of oligodendrocytes. Myelin instability in multiple sclerosis (MS) is associated with the loss of positive charge in MBP as a result of posttranslational enzymatic deimination. A highly-conserved central membrane-binding fragment (murine N81-PVVHFFKNIVTPRTPPP-S99, identical to human N83-S101) represents a primary immunodominant epitope in MS. Previous low-resolution electron paramagnetic resonance measurements on the V83-T92 fragment, with Cys-mutations and spin-labeling that scanned the epitope, were consistent with it being a membrane-associated amphipathic α-helix. Pseudodeimination at several sites throughout the protein, all distal to the central segment, disrupted the α-helix at its amino-terminus and exposed it to proteases, representing a potential mechanism in the autoimmune pathogenesis of MS. Here, we have used magic-angle spinning solid-state NMR spectroscopy to characterize more precisely the molecular conformation and dynamics of this central immunodominant epitope of MBP in a lipid milieu, without Cys-substitution. Our solid-state NMR measurements have revealed that the α-helix present within the immunodominant epitope is shorter than originally modeled, and is independent of the pseudodeimination, highlighting the importance of the local hydrophobic effects in helix formation and stability. The main effect of pseudodeimination is to cause the cytoplasmic exposure of the fragment, potentially making it more accessible to proteolysis. These results are the first, to our knowledge, to provide atomic-level detail of a membrane-anchoring segment of MBP, and direct evidence of decreased MBP-membrane interaction after posttranslational modification.

INTRODUCTION

The myelin sheath is a multilamellar lipid membrane surrounding nerve axons in both the central and peripheral nervous systems (Fig. 1). Myelin basic protein (MBP) is a major protein component of the sheath in the brain and spinal cord. Its primary role is to maintain the compaction of myelin through peripheral association with the apposing cytoplasmic faces of the oligodendrocyte membrane (1–3) (Fig. 1). It is an intrinsically disordered protein which also interacts with many other proteins and ligands such as actin, tubulin, calmodulin, and SH3-domain containing proteins, thus potentially acting as a linker in structural and signaling networks (1,4–7).

The 18.5 kDa splice isoform of MBP is the most abundant in the adult human brain, and exists, due to a diversity of posttranslational modifications, as a number of charge components known as C1–C8, with net positive charge decreasing from +19 to <+13 at pH 7.0. Component C1 is the least modified, most cationic, and the most abundant variant in healthy adult myelin. Component C8 is characterized primarily by the enzymatic deimination of arginine to citrulline, reducing its net positive charge. The C8 component is found in elevated levels both in developing myelin in infants and in adults with the human inflammatory demyelinating disease multiple sclerosis (MS) (8,9). Our previous studies have used recombinant murine variants of these components, namely, unmodified rmC1 and pseudodeiminated rmC8 (Fig. 2), which are almost identical to the human forms (6,7), and which have properties similar to the natural proteins' forms C1 and C8 (10,11).

MBP adopts an extended conformation in aqueous solution, but gains local secondary structure upon interacting with binding partners, and in particular with lipids, which interaction is the focus of this article. The current portrayal of membrane-associated MBP derived from electron paramagnetic resonance (EPR) and solid-state NMR (SSNMR) measurements is depicted in Fig. 1. Hydrophobic moment analysis of the amino-acid sequence of MBP suggests the existence of three strongly amphipathic α-helices in the protein (12), located in the N- and C-termini and in the central region (Fig. 1 *C*). EPR measurements of the rmC1 variant (with single Cys-substitutions and spin labels distributed across the protein) have indicated that these regions are, indeed, embedded into the lipid membrane (13). Detailed EPR measurements of the central region comprising residues Pro^{82}-Pro^{93} (murine 18.5 kDa sequence numbering), which represents the primary immunodominant epitope, were indeed consistent with this segment being an amphipathic α-helix lying on the membrane surface (14). Subsequent EPR measurements conducted on a pseudodeiminated MBP variant (1) further

Submitted May 18, 2010, and accepted for publication June 14, 2010.

*Correspondence: gharauz@uoguelph.ca or vladizha@uoguelph.ca

Mumdooh A. M. Ahmed's present address is Department of Physics, Faculty of Science at Suez, Suez Canal University, Suez, Egypt.

Editor: Marc Baldus.

0006-3495/10/08/1247/9 $2.00

doi: 10.1016/j.bpj.2010.06.022

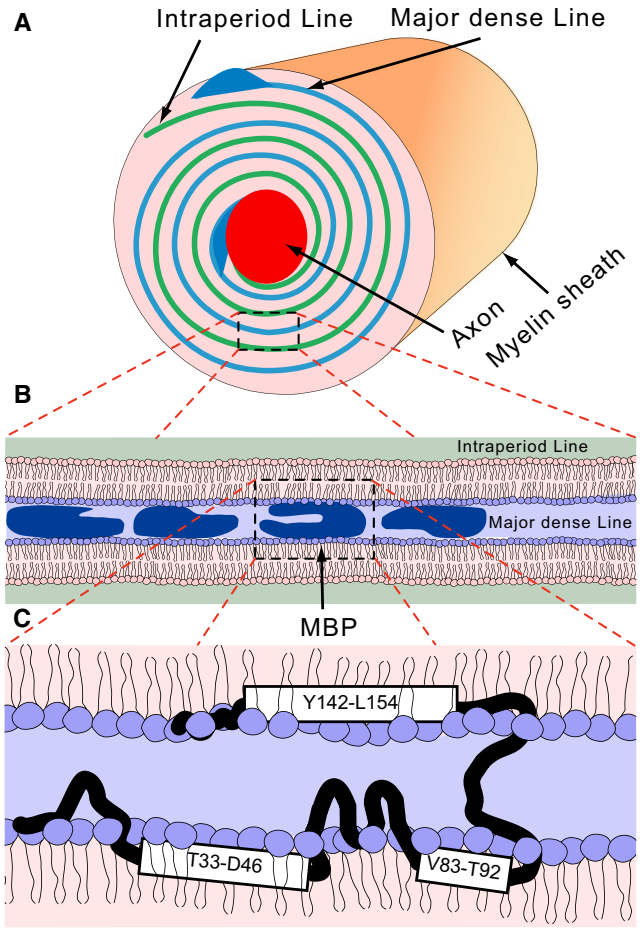

FIGURE 1 (*A*) Structure of the myelin sheath. (*B*) The myelin sheath consists of stacked lipid bilayers. Myelin basic protein peripherally binds the adjacent leaflets on the cytoplasmic side and acts as an adhesive protein. (*C*) There are three potential amphipathic helices in MBP shown in the figure, which may peripherally interact with lipids and represent putative lipid binding domains. The details of protein-lipid binding are not known, and the arrangement shown in this figure is one out of many possibilities.

confirmed that the rmC8 variant was less-strongly associated with membranes along its C-terminal and central regions (13). In particular, the central fragment formed a two-residues' shorter α-helix comprising residues H85-T92 that was also more exposed (to proteases such as cathepsin D, for example) (15,16).

In this study, we have used magic-angle spinning (MAS) solid-state NMR (SSNMR) spectroscopy to determine the molecular conformation and to characterize the dynamics of the central immunodominant epitope of MBP in lipid milieu. Our SSNMR measurements did not require site-specific Cys-substitution and labeling, and have confirmed that the immunodominant epitope adopts an α-helical conformation, but that the helix appears to be approximately one-turn shorter than originally believed. Pseudodeimination does not affect the helical structure. However, it does cause the exposure of the epitope to solvent, making it more accessible to proteolysis.

```
                10        20        30        40        50
rmC1: ASQKRPSQRS KYLATASTMD HARHGFLPRH RDTGILDSIG RFFSGDRGAP
rmC8: ASQKRPSQRS KYLATASTMD HAQHGFLPRH QDTGILDSIG RFFSGDRGAP
                60        70        80        90        100
rmC1: KRGSGKDSHT RTTHYGSLPQ KSQHGRTQDE NPVVHFFKNI VTPRTPPPSQ
rmC8: KRGSGKDSHT RTTHYGSLPQ KSQHGRTQDE NPVVHFFKNI VTPRTPPPSQ
               110       120       130       140       150
rmC1: GKGRGLSLSR FSWGAEGQKP GFGYGGRASD YKSAHKGFKG AYDAQGTLSK
rmC8: GKGRGLSLSR FSWGAEGQQP GFGYGGQASD YKSAHKGFKG AYDAQGTLSK
               160       170
rmC1: IFKLGGRDSR SGSPMARRLE HHHHHH
rmC8: IFKLGGQDSR SGSPMAQQLE HHHHHH
```

FIGURE 2 Amino-acid sequences of recombinant murine 18.5 kDa rmC1 and rmC8 MBP variants. (*Dashed rectangles*) Gln substitutions (pseudodeimination) performed to produce rmC8. The highlighted region is the fragment examined here using MAS-SSNMR.

MATERIALS AND METHODS

Protein overexpression, isotopic labeling, and purification

Materials were as described previously (17) and in the Supporting Material. The unmodified classic 18.5 kDa recombinant murine myelin basic protein (rmC1), and its pseudodeiminated variant (rmC8), were expressed in *Escherichia coli* BL21-CodonPlus(DE3)-RP cells (Stratagene, La Jolla, CA) and purified as described previously (10,11). The 18.5 kDa isoform of MBP contains only three valines at the positions V83, V84, and V91, and two asparagines at N81 and N89. All these residues are located within the immunodominant epitope or in its immediate vicinity (Fig. 2). Detection of Val and Asn resonances can be used to study the secondary structure and dynamics of the epitope. The [U-^{13}C,^{15}N-Val,Asn, U-^{15}N]-labeled recombinant murine C1 (rmC1-NV) protein for SSNMR spectroscopy was derived from cells grown in M9 medium supplemented with uniformly ^{13}C,^{15}N-labeled Asn and Val at 1 mM, along with $^{15}NH_4Cl$ and natural abundance glucose. The [U-^{13}C,^{15}N-Val,Asn, U-^{15}N]-labeled recombinant murine C8 form (rmC8-NV) was prepared with the addition of labeled amino acids at 0.5 mM. Selective labeling of the Val and Asn residues in rmC1 and rmC8 was optimized as described in the Supporting Material. For both samples, the labeled amino acids were added to the growing bacterial culture 1 h before isopropyl-β-*d*-thiogalactopyranoside induction.

Preparation of samples for solid-state NMR spectroscopy

The procedures for making large unilamellar vesicles (LUVs) were adapted from previous investigations (13–15,17). Briefly, dry lipid powders were mixed at the desired molar ratios (see Table 1 for details on the samples used), and dissolved in a 2:1:1 (vol %) mixture of methanol/chloroform/ddH_2O. The organic solvent was then dried under a stream of nitrogen gas, followed by an overnight drying under vacuum. The lipids were rehydrated by vigorous shaking overnight with two freeze-thaw cycles in a buffer containing 2 mM HEPES-NaOH, 100 mM NaCl, and 1 mM EDTA, at pH 7.6. A mini-extruder (Avanti Polar Lipids, Alabaster, AL) was used to extrude the hydrated lipid mixture through a 100-nm polycarbonate filter. To ensure a uniform size distribution of the lipid vesicles, a minimum of 35 extrusion cycles was employed, resulting in lipid vesicles of ~100-nm diameter as confirmed by dynamic light scattering. The concentration of lipids in the final preparation after extrusion was estimated using a phosphorus assay (18,19).

The typical reconstitution procedure was as follows. Protein and LUVs were diluted in the same buffer (2 mM HEPES-NaOH, 100 mM NaCl, and 1 mM EDTA at pH 7.6) to a final concentration of 0.5 mg/mL. Aliquots of protein and lipid stocks were loaded into a 2 mL microfuge tube, mixed by inversion, and incubated at room temperature for 2 h. The protein/lipid aggregates were then collected by centrifugation at 18,000 $\times$ *g* for 2 h.

TABLE 1 Lipid compositions of LUVs and *P/L*s of samples used for examination of protein-lipid vesicle aggregation conditions

Sample	Protein	Lipid composition (molar ratio)	Initial *P/L* (mass ratio)	Final *P/L* (mass ratio)	m_f (mg)*
A	rmC1	1:1 DMPG/DMPC	1:1	1:1.7	0.8
B	rmC1	1:4:5 DMPC/Chol/DMPG	1:2	1:1.8	0.8
C	rmC1	1:1 DMPG/DMPC	1:2	1:1.6	4.5†
D	rmC8	1:1 DMPG/DMPC	1:2	1:2.5	6.0†
E	rmC8	1.5:8.5 DMPG/DMPC	1:6	1:6	0.8

LUVs, large unilamellar vesicles; P/L, protein/lipid ratio.
*m_f, final protein content in solid-state (SSNMR) samples.
†For *P/L* aggregation and preliminary SSNMR testing, small-scale samples have been used; the final protein content reported in this table is for our final samples used throughout the remaining studies.

The supernatants and pellets were separated and the protein and lipid contents were estimated using the standard bicinchoninic acid and phosphorus assays (18–21), respectively, as described previously (17). The pellets obtained were then center-packed into a standard 3.2-mm MAS rotor for examination using SSNMR. ^{31}P measurements conducted previously confirmed the lamellar phase of lipids (17).

After several SSNMR investigations on reconstituted MBP/LUV samples with different lipid compositions and initial protein/lipid mass ratios, as described in Results and Discussion, we determined that the epitope conformation was independent of the protein/lipid and 1,2-dimyristoyl-*sn*-glycero-3-phosphocholine (DMPC) to 1,2-dimyristoyl-*sn*-glycero-3-[phospho-*rac*-(1-glycerol)]) (DMPG) ratios. Our final rmC1 sample was prepared from 1:1 (molar ratio) DMPG/DMPC large unilamellar vesicles (LUVs) mixed with protein at a 1:2 initial protein/lipid mass ratio. The protein-lipid aggregate was collected by ultracentrifugation at 100,000 × *g* for 80 min. Approximately 4.5 mg of rmC1 (1:46 protein/lipid molar ratio) was thus packed in a 3.2-mm rotor.

The less positively-charged rmC8 variant (+13 compared to +19 for rmC1) had a naturally reduced tendency to aggregate lipid vesicles, which resulted in the reduction of protein content in the lipid aggregate. The preparation procedure was similar to that of rmC1, but we used larger initial amounts of protein and lipid: 9 mg of protein dissolved in 18 mL of buffer, and 18 mg of lipids diluted in 36 mL of buffer, were mixed. Approximately 6 mg (1:72 protein/lipid molar ratio) of rmC8 was packed into a thin-walled 3.2-mm MAS rotor (Bruker BioSpin, Billerica, MA). Both samples were fully hydrated as evident, for example, from the presence of a strong water line in the proton NMR spectra (data not shown), as well from our previously published water-MBP correlation spectra (17).

Solid-state NMR spectroscopy and secondary structure propensities

All experiments were performed on Avance III spectrometers (Bruker Optics, Billerica, MA) operating at 600.13 and 800.23 MHz proton frequencies, and equipped with a triple-resonance ^{1}H-^{13}C-^{15}N 3.2 mm E-Free MAS probe (Bruker BioSpin) (22). The one-dimensional ^{13}C spectra were collected using either the ramped version of cross-polarization (CP) (23), followed by an SPC5$_3$-based double-quantum filter (DQF) (24,25) used to eliminate the natural abundance ^{13}C signal arising both from lipids and unlabeled parts of the protein, or through-bond insensitive nuclear enhancement by polarization transfer (INEPT) (26) excitations.

The two-dimensional ^{13}C-^{13}C correlation spectra were recorded using through-space (dipolar-assisted-rotational resonance, or spin diffusion) transfer mechanisms (27). All ^{13}C-^{13}C correlation spectra were acquired at a MAS rate of 12 kHz and with a recycle delay of 1.9 s. All pulse sequences were modified to start with ^{1}H/^{13}C CP and a $\pi/2$ ^{13}C pulse to ensure that both mobile and immobile parts of the protein were excited with maximum efficiency. The one-dimensional (CON)CA and (CANCO)CA spectra and two-dimensional ^{13}C-^{15}N N(CA)CX and (CO)N(CO)CA correlation spectra were collected at 240 K. Typical field strengths were 80 kHz for small-phase-incremental-alteration-heteronuclear-dipolar-decoupling-scheme-with-64-composite-pulses (SPINAL-64) decoupling (28), and 42 kHz, 30 kHz, and 90 kHz for ^{13}C, ^{15}N, and ^{1}H fields, respectively, during ^{15}N/^{13}C CP. Typical 90° pulse lengths used were 2.78 μs, 5 μs, and 6 μs for proton, carbon, and nitrogen, respectively. Additional experimental details are given in Table S1 and Table S2 in the Supporting Material.

All two-dimensional spectra were processed with NMRPipe (29) using $\pi/2$-shifted sine-squared apodization for both dimensions before Fourier transformation. Carbon chemical shifts were indirectly referenced to 2,2-dimethyl-2-silapentane-5-sulfonic acid through the ^{13}C adamantane downfield peak resonating at 40.48 ppm (30). Nitrogen chemical shifts were referenced indirectly by using the ratio of $\gamma_N/\gamma_C = 0.402979946$ (31). All temperature values reported here represent sample temperatures.

The chemical shift deviations were used to assess the secondary structure propensities along the backbone of both rmC1 and rmC8 within the assigned residues (32,33). Random coil values (34) were corrected for sequence dependence (35). We used the C^{α} secondary shifts only, because they were the least sequence-dependent of all resonances.

RESULTS AND DISCUSSION

Sample reconstitution—protein labeling and choice of lipid composition

Two samples were analyzed by one- and two-dimensional SSNMR spectroscopy:

1. Unmodified [U-^{13}C,^{15}N-Val,Asn, U-^{15}N]-MBP (rmC1-NV, recombinant murine C1 form).
2. Pseudodeiminated [U-^{13}C,^{15}N-Val,Asn, U-^{15}N]-MBP (rmC8-NV, recombinant murine C8 form).

The amino-acid sequences of both proteins are shown in Fig. 2. We have previously shown that rmC1 has similar properties to the natural brain-derived C1 form, in particular lipid aggregation properties (11). The rmC8 variant differs from rmC1 by six citrulline-mimicking substitutions (R23Q, R31Q, K119Q, R127Q, R157Q, and R168Q), which reduce the overall positive charge of the protein, and which have been shown to result in similar membrane- and protein-interaction properties to the natural C8 component (12,36).

Our previous SSNMR studies of MBP have shown an overall high degree of mobility of the protein in the lipid environment (17). In INEPT-based experiments specifically optimized for detection of mobile fragments, the central region (residues K68–K102) containing the lipid-bound central epitope could not be observed. As mentioned previously, both Asn and all three Val residues in the entire protein are in or adjacent to the immunodominant epitope (Fig. 2). We thus labeled these residues selectively with ^{13}C, and the whole protein uniformly with ^{15}N, after optimization as described in Supporting Material.

The myelin sheath in the central nervous system is a complicated mixture of lipids, and includes phospholipids with negatively-charged headgroups (13% of phosphatidylserine and 2% of phosphatidylinositol, molar

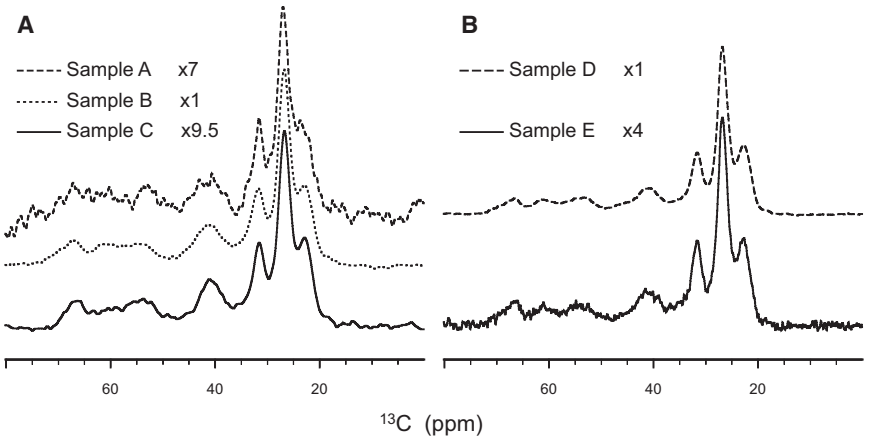

FIGURE 3 The one-dimensional ^{13}C spectra for rmC1 and rmC8 reconstituted in membranes of different lipid compositions and at different *P*/*Ls*. (*A*) The CPMAS DQF spectra for three rmC1 samples *A*–*C* (Table 1). (*B*) The CPMAS DQF spectra for two rmC8 samples *D* and *E* (Table 1). All spectra were acquired at −25°C and processed with a 100-Hz exponential window function before Fourier transformation. The spectra are scaled as indicated by the multiplication factors in both panels to bring them to equal heights for better visual comparison.

ratio), with neutral headgroups (27% of phosphatidylethanolamine and 11% of phosphatidylcholine), sphingomyelin (3%), and cholesterol (44%) (37). Many of these lipids have unsaturated bonds, which are not stable on the timescale of a typical SSNMR experiment. Thus, we also evaluated the effects of lipid composition on protein conformation.

For initial evaluations of conditions, five LUV samples (*A*–*E*) were prepared with lipids of different types, varying proportion of charged lipids, and with various protein/lipid (*P*/*L*) ratios to test the effect of lipid composition and *P*/*L* on the MBP conformation (Table 1). For sensitivity considerations, we only collected one-dimensional spectra in these preliminary trials. Although these experiments did not permit detailed site-specific assessment, we expected that any spectral changes would serve as an indicator of large conformational rearrangements induced by lipids or by high protein/lipid ratio.

Fig. 3 *A* compares a series of DQF spectra of rmC1 obtained in different lipid compositions (Table 1, samples *A*–*C*). In these spectra, we observed signals from labeled amino acids in the protein, primarily asparagines and valines located in the immunodominant epitope of MBP, as well as contributions from scrambled amino acids (only pairs of directly bonded ^{13}C atoms contributed to the DQF signal). All DQ-filtered spectra collected at −25°C were practically identical for all three systems, implying that the change of lipid composition and protein/lipid had minimal effect on the conformation of membrane-associated rmC1.

Fig. 3 *B* examines the effect of lipid composition and of protein/lipid ratios on rmC8 (Table 1, samples *D* and *E*). The appearance of the DQF spectrum is again identical for both samples, and is also similar to the DQF spectra of rmC1 in Fig. 3 *A*. Thus, these spectra indicate that at low temperature the conformations of labeled residues, primarily Val and Asn, are independent of the lipid composition, protein/lipid ratio, and the overall charge of the protein. In the following experiments, we have chosen samples with 1:1 DMPG/DMPC LUVs as a stable model (on the timescale of SSNMR experiments) to mimic the myelin sheath composition.

SSNMR spectra identify the presence of a short α-helical structure within the epitope in both unmodified and pseudodeiminated forms

Site-specific assignments of backbone ^{13}C and ^{15}N resonances in Val and Asn residues were obtained using a combination of spectral-edited one-dimensional spectra and two-dimensional ^{13}C-^{13}C correlation spectroscopy. The initial set of measurements was conducted at −25°C. Possible conformational changes induced by temperature-dependent lipid phase transition were studied by following a gradual change in peak positions in the two-dimensional ^{13}C-^{13}C spectra.

The C^{α} resonances of Val^{83} and Val^{84} were assigned using one-dimensional edited experiments (CON)CA and (CANCO)CA, in which polarization was transferred in a number of selective transfer steps between two sequentially labeled residues. Because Val^{83}-Val^{84} was the only pair of sequentially labeled amino acids (Fig. 2), the (CON)CA and (CANCO)CA experiments allowed selective observation of the $Val^{83}C^{\alpha}$ and $Val^{84}C^{\alpha}$ peaks. The corresponding spectra are shown in Fig. 4 *A*, where the $Val^{83}C^{\alpha}$ and $Val^{84}C^{\alpha}$ peaks are clearly visible above the background of resonances from residually labeled carbon atoms.

Of the two asparagines in the MBP sequence, only Asn^{81} precedes proline (Fig. 2). The $Asn^{81}C^{\alpha}$ peak was assigned from the two-dimensional (CO)N(CO)CA spectrum. The H-C′-N excitation was found to be more efficient for the excitation of the proline backbone ^{15}N resonance than the direct H-N transfer. The (CO)N(CO)CA spectrum in Fig. 4 *B* shows a pronounced peak at 137.6/52.1 ppm, which corresponds to a $Pro^{82}N/Asn^{81}C^{\alpha}$ correlation.

The assignments for the remaining Val^{91} and Asn^{89} were obtained from the two-dimensional ^{13}C-^{13}C dipolar-assisted-rotational resonance correlation spectrum shown in Fig. 4 *C*. The spectrum displays three peaks in a valine C^{α}/C^{β} fingerprint region centered at ~F_1/F_2 of 64/32 ppm. The already assigned Val^{83} and Val^{84} C^{α} resonances result in two overlapping peaks at F_1/F_2 of 66.6/31.5 ppm. The third valine correlation at F_1/F_2 of 62.3/32.1 ppm

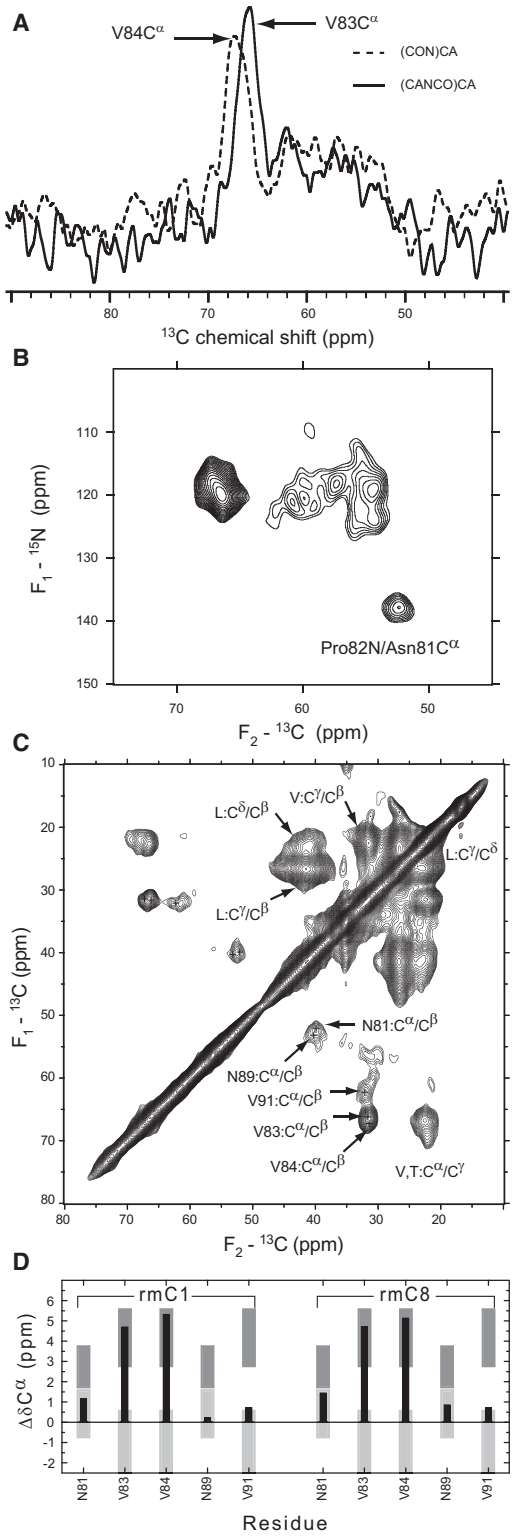

FIGURE 4 (*A*) One-dimensional ^{13}C (CON)CA and (CANCO)CA spectra used to assign the C^{α} peaks of both Val^{83} and Val^{84} in membrane-associated rmC1. Both spectra were acquired at −25°C and processed with 100-Hz exponential line broadening before Fourier transformation. Because there is only one isotopically labeled pair of adjacent residues in the rmC1 and rmC8 sequences, both spectra should ideally display only one peak each. Because of scrambling during selective-labeling, there are many other overlapping residues that show up in the range from 52 to 62 ppm. (*B*) Two-dimensional (CO)NCOCA correlation spectrum allowing identification of the $Asn^{81}C^{\alpha}$ chemical shift. (*C*) Two-dimensional 600 MHz ^{13}C-^{13}C correlation spectrum of membrane-associated rmC1 recorded at −25°C. (*D*) Sequence-corrected chemical shift deviations of C^{α} atoms of membrane-associated rmC1 and rmC8, at −25°C (shown in *black*). (*Dark shaded bars*) One standard deviation of α-helical $\Delta\delta C^{\alpha}$ shifts. (*Light shaded bars*) One standard deviation of β-sheet $\Delta\delta C^{\alpha}$ shifts.

corresponds to Val^{91}. Because of the low degree of ^{13}C labeling of proline (~18% as evident from solution NMR results discussed in Supporting Material), we ruled out the possibility that these cross-peaks could also be due to Pro C^{α}/C^{β} correlations.

Similarly, the correlation at F_1/F_2 at ~52.7:40.5 ppm corresponds to the asparagine C^{α}/C^{β} correlations. The volume of this peak is approximately equal to that of the Val^{83}/Val^{84} C^{α}/C^{β} overlapping correlations, and is approximately two-times larger than the assigned Val^{91} C^{α}/C^{β} cross-peak. Thus, despite its appearance as a single peak, it likely results from two asparagines, Asn^{81} and Asn^{89}. One of these resonances has already been assigned to Asn^{81} from the (CO)N(CO)CA experiment, and the other must be due to Asn^{89}, as both Leu and Asp (the other possible candidates) showed very low levels of labeling at C^{α} positions.

A similar set of experiments on the reduced charge variant rmC8 resulted in nearly identical chemical shifts for Asn^{81}, Val^{83}, Val^{84}, Asn^{89}, and Val^{91}, in complete agreement with nearly identical DQF one-dimensional spectra of these two samples. Thus, our results indicate that at low temperature, the Asn^{81}-Thr^{92} fragment adopts a very similar overall conformation in both rmC1 and rmC8.

We finally note that the two-dimensional ^{13}C-^{13}C correlation spectrum (Fig. 4 *C*) shows a large number of additional cross-peaks between residually labeled carbon atoms of most of the residues. The most pronounced are those corresponding to Leu side-chain C^{β}/C^{γ} correlations at ~F_1/F_2 of 41.4/26.6 ppm, C^{γ}/C^{δ} correlations at F_1/F_2 of 26.6/22.7 ppm, and C^{β}/C^{δ} correlations at F_1/F_2 of 41.4/22.7 ppm. As discussed in the Supporting Material, we do not expect any Leu correlations involving C^{α}, as these atoms remain unlabeled. Some Val C^{α}/C^{γ} and Thr C^{β}/C^{γ} correlations are also detected at ~F_1/F_2 of 67.1/22.4 ppm. These residual cross-peaks do not interfere with the Val and Asn correlations of interest.

NMR chemical shifts are sensitive reporters on local secondary structure. We used C^{α} chemical shifts of the assigned residues to compare the backbone conformation of the immunodominant epitope for both rmC1 and pseudo-deiminated rmC8 reconstituted systems. The C^{α} secondary shifts (i.e., the differences between the experimentally determined chemical shifts and their random coil values) for both rmC1 and rmC8 at −25°C are shown in Fig. 4 *C*. Overall, the plot demonstrates clearly that the immunodominant epitope

adopts a very similar conformation in both protein variants. The C^{α} secondary shifts of both Val^{83} and Val^{84} are strongly positive, of ~5 ppm, indicating their strongly helical conformations. The Val^{83}-Val^{84} pair is only three residues' away from a strongly hydrophobic Phe^{86}-Phe^{87} pair, and both pairs likely face the hydrophobic core of the bilayer (14). On the other hand, Val^{91} and both Asn^{81} and Asn^{89} have only slightly positive secondary chemical shifts, and define the helical boundaries for the epitope. We therefore conclude that the α-helix likely comprises residues Val^{83}-Lys^{88} in both rmC1 and rmC8 variants, and its structure in this environment is unaffected by the pseudodeimination at sites distal to it.

Secondary structure and dynamics of the epitope in the lipid fluid phase

The depth of penetration of MBP fragments into a lipid bilayer may depend not only on protein properties such as local hydrophobicity and overall charge, but also on the state of the lipids (1,13). In particular, MBP may preferentially bind the fluid domains of the membrane (38), and can be squeezed out of the membrane when lipids are in the gel phase. To obtain structural and dynamic information on the behavior of the epitope region of the protein at different lipid states, we collected a series of two-dimensional ^{13}C-^{13}C correlation spectra in the temperature range from $-25^{\circ}C$ to $35^{\circ}C$. The resonance assignments of all $^{13}C^{\alpha}$ shifts were obtained by tracking the gradual change in cross-peak positions as a function of temperature. As we reported previously, solvent-exposed fragments of MBP are highly dynamic. Although the membrane-associated immunodominant epitope is significantly less mobile than the solvent-exposed parts, it too experiences dynamic motions, which result in effective attenuation of dipole-dipole interactions and consequently in the reduction of cross-peaks intensities in the dipolar based correlation spectra. Nonetheless, the observed correlations allow us to draw conclusions about the temperature-induced effects.

The overall structure of carbon-carbon correlation spectra remained unchanged: both Asn and Val C^{α}/C^{β} correlations remained pronounced, albeit of reduced amplitudes. The ratio between Val and Asn C^{α}/C^{β} peak volumes was ~3:2 throughout the entire probed temperature range in accordance with the expected number of correlations, suggesting that all the observed residues in the epitope are subjected to the same dynamics. Although these observations are of a semiquantitative nature, they indicate that all three valines and two asparagines can be observed in the spectra.

On the other hand, while an overall two-dimensional shape of Val C^{α}/C^{β} cross peaks does not change (Fig. 5 *A*), we have observed significant redistribution of peak intensities in this region in both rmC1 and rmC8 samples. Specifically, the intensity of the Val^{83}/Val^{84} overlapping correlation decreases, while the intensity of Val^{91} increases (Fig. 5 *B*),

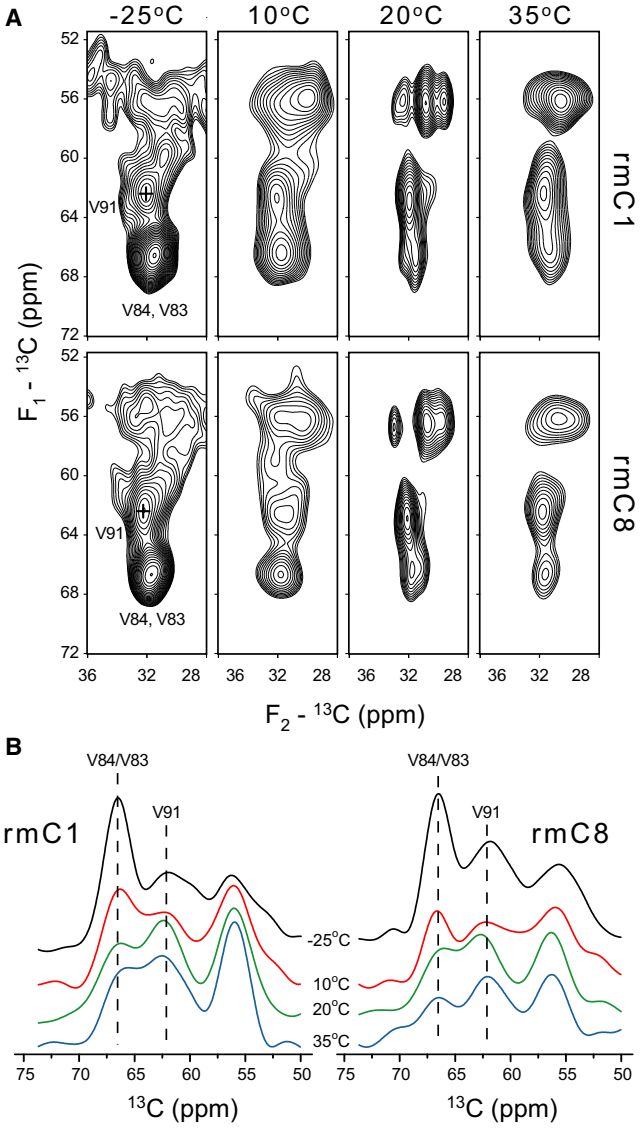

FIGURE 5 (*A*) The Val C^{α}/C^{β} correlation region of a ^{13}C-^{13}C correlation spectrum as a function of temperature. V91 and V83 positions and V84 correlations are shown in the low temperature spectrum. (*B*) Projections of carbon correlations in the Val C^{α}/C^{β} region for both rmC1 and rmC8 at all four temperatures, showing redistribution of intensities from the Val^{83}/Val^{84} C^{α} to the Val^{91} C^{α} region.

indicating possible conformational rearrangements within the epitope—for example, changes in conformation of V83 and/or V84. Although the assignment of Val^{83} and Val^{84} C^{α} resonances is ambiguous at high temperature, we note that Val^{83} is more likely to undergo stronger changes, as it is located at the N-terminal end of the helix.

Mobility of the immunodominant epitope in rmC1 and rmC8

The line widths of C^{α} and C^{β} resonances of the epitope residues remained heterogeneously broadened on the order of 2

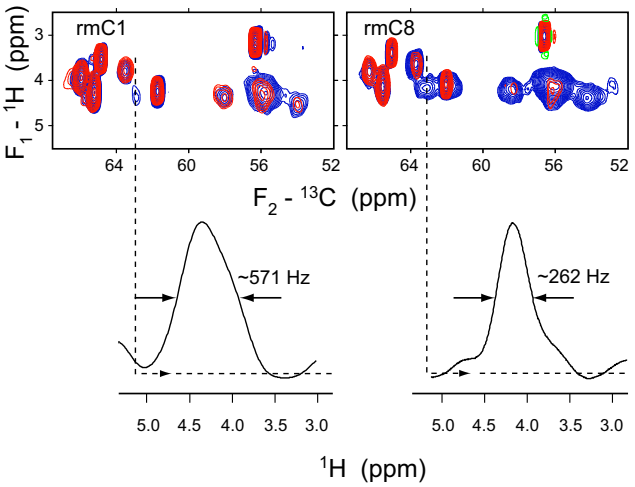

FIGURE 6 Two-dimensional ^{1}H-^{13}C INEPT heteronuclear chemical-shift correlation spectra in [^{13}-C-Asn,Val,U-^{15}N]-labeled rmC1 and rmC8. (*Red spectra*) Samples with unlabeled protein, showing lipid correlations. The one-dimensional ^{1}H traces at the position of V91C$^{\alpha}$ are shown at the bottom for both spectra.

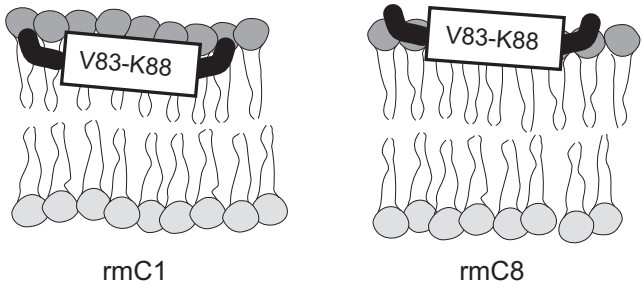

FIGURE 7 The immunodominant epitope adopts a similar α-helical molecular conformation in both rmC1 and rmC8 proteins. The α-helix is more exposed in rmC8, as follows from the dynamic information derived from the measurements of proton line widths.

ppm in both rmC1 and rmC8. Thus, the conformational motions were unable to average this heterogeneity. Additional evidence of strong motions in rmC1 and rmC8 was derived from proton-carbon heteronuclear chemical-shift correlation spectra recorded at 35°C using INEPT (through-bond) and ramped CP (through-space) as mixing methods. Both methods yielded similar correlation patterns as shown for the case of INEPT in Fig. 6 for both Asn and Val-labeled rmC1 and rmC8 samples, along with the spectra of samples prepared with natural abundance rmC1 and rmC8 proteins. The correlations from natural abundance protein samples result only from lipids and help identify the protein-specific signals, which could be assigned by simply matching ^{13}C shifts. In particular, the Val^{91} C$^{\alpha}$/H$^{\alpha}$ correlation is clearly distinguished in both samples. The proton line-width of this peak in rmC1 is ~570 Hz (Fig. 6), dramatically reduced compared to a typical ^{1}H line-width in rigid solids where dipolar broadening is approximately tens of kilohertz (39). This line-width reduction indicates the presence of extensive molecular motions. The proton line-width of Val91 in rmC8 becomes even smaller than in rmC1, ~260 Hz, indicating a further increase in mobility. Thus, the immunodominant epitope appears to be less motionally restricted in rmC8, despite having a very similar molecular conformation.

SIGNIFICANCE AND CONCLUSIONS

Multiple sclerosis (MS) is a human demyelinating disease of multifactorial origin. The severity of the disease has been correlated with elevated levels of the C8 component of MBP, which is the least cationic of all MBP variants. An overall charge reduction in deiminated forms of MBP has an effect on the protein/lipid interactions strengths, and may be responsible for modulating the compactness of the myelin sheath. The importance of understanding of MBP-lipid interactions has prompted numerous structural studies of MBP and of its lipid-binding domains. Extensive biochemical and biophysical studies have revealed that the least-modified C1 component of MBP contains three lipid-binding fragments: in addition to the immunodominant epitope studied in this work, two additional fragments are located in the C- and N-termini, while the remaining parts of the protein remain solvent-exposed, mobile, and unstructured.

The main finding of this study, shown in Fig. 7, is that the immunodominant epitope contains a short α-helix encompassing residues Val^{83}-Lys^{88} in both rmC1 and rmC8 MBP variants (which may even be shorter at physiologically relevant temperatures), and is not sensitive to the overall electrostatic charge of the protein in this reconstituted system. Indeed, the nearest deimination site to the immunodominant epitope is at the position of 119 where Lys^{119} in rmC1 is replaced by Q119 in rmC8 (Fig. 2). This site is 25 residues away from the epitope. Given that MBP remains mobile and largely unstructured in lipids, we expect that the K119Q substitution would have a minimal effect on the helix. Instead, the secondary structure is governed by the strong local hydrophobic interactions between the core of the lipid bilayer and the nonpolar face of the helix (V83–V84 and F86–F87 pairs) (14). On the other hand, the increased dynamics of the epitope in rmC8 points to the importance of electrostatic interactions, and is consistent with it being more exposed to the exterior of the membrane, although this exposure has no significant effect on the local secondary structure.

Our observation of only a short helical six-residue-long structure is somewhat in disagreement with previous site-directed spin-labeling (SDSL)/electron-paramagnetic resonance (EPR) measurements, which were consistent with the presence of a longer helix within the epitope. Site-directed mutagenesis to Cys required for SDSL/EPR may introduce some structural distortions to the protein in

its membrane-associated form. Furthermore, ambiguity of the cysteine side-chain conformation and preferential partitioning of the paramagnetic label into a lipid bilayer or solvent may introduce additional complication to the interpretation of SDSL/EPR data. Our results, on the other hand, are based on the measurements conducted in intact rmC1 and rmC8.

Another possible reason for disagreement between EPR and NMR results may be related to the difference in lipid composition and protein/lipid used in the measurements. The EPR experiments were performed on proteins reconstituted at a 10-fold lower protein/lipid, with lipid vesicles comprising roughly 18% (mol) charged lipids. In this study, the higher percentage of charged lipids (50 mol %) may have resulted in a stronger overall electrostatic interaction of both the rmC1 and rmC8 variants with the membrane. Although our control experiments indicate that these factors play a minor role in the formation of the epitope secondary structure at low temperature (Fig. 3), they will certainly affect the dynamic properties of the proteins and may become important at higher temperatures. Investigations of the effects of lipid composition on the MBP dynamics and structure are currently underway.

SUPPORTING MATERIAL

One figure and three tables are available at http://www.biophysj.org/biophysj/supplemental/S0006-3495(10)00734-4.

We are grateful to Ms. Valerie Robertson and Mr. Peter Scheffer of the University of Guelph NMR Centre for technical support, and to Drs. Joan Boggs and Leonid Brown for helpful discussions and comments on the manuscript.

This work was supported by the Canadian Institutes of Health Research (operating grant No. MOP 74468 to G.H. and V.L.), the Canada Foundation for Innovation, and the Ontario Innovation Trust. V.L. is a Tier II Canada Research Chair in Biophysics, and a recipient of an Early Researcher Award from the Ontario Ministry of Research and Innovation. M.A. was initially a recipient of a Doctoral Studentship from the Ministry of Higher Education and Scientific Research of Egypt. V.V.B. was the recipient of a Postdoctoral Fellowship from the Multiple Sclerosis Society of Canada.

REFERENCES

1. Boggs, J. M., I. R. Bates, …, G. Harauz. 2008. Interactions of the 18.5 kDa myelin basic protein (MBP) with lipid bilayers—studies by electron paramagnetic resonance (EPR) spectroscopy and implications for generation of autoimmunity in multiple sclerosis. *In* Myelin Basic Protein. J. M. Boggs, editor. Nova Science, New York.
2. Hu, Y., I. Doudevski, …, J. Israelachvili. 2004. Synergistic interactions of lipids and myelin basic protein. *Proc. Natl. Acad. Sci. USA.* 101:13466–13471.
3. Min, Y., K. Kristiansen, …, J. Israelachvili. 2009. Interaction forces and adhesion of supported myelin lipid bilayers modulated by myelin basic protein. *Proc. Natl. Acad. Sci. USA.* 106:3154–3159.
4. Boggs, J. M. 2006. Myelin basic protein: a multifunctional protein. *Cell. Mol. Life Sci.* 63:1945–1961.
5. Boggs, J. M. 2008. Myelin basic protein interactions with actin and tubulin in vitro—binding, assembly, and regulation. *In* Myelin Basic Protein. J. M. Boggs, editor. Nova Science, New York.
6. Harauz, G., N. Ishiyama, …, C. Farès. 2004. Myelin basic protein-diverse conformational states of an intrinsically unstructured protein and its roles in myelin assembly and multiple sclerosis. *Micron.* 35:503–542.
7. Harauz, G., and D. S. Libich. 2009. The classic basic protein of myelin-conserved structural motifs and the dynamic molecular barcode involved in membrane adhesion and protein-protein interactions. *Curr. Protein Pept. Sci.* 10:196–215.
8. Moscarello, M. A., F. G. Mastronardi, and D. D. Wood. 2007. The role of citrullinated proteins suggests a novel mechanism in the pathogenesis of multiple sclerosis. *Neurochem. Res.* 32:251–256.
9. Mastronardi, F. G., and M. A. Moscarello. 2008. Deimination of MBP by PAD enzymes, and their role in multiple sclerosis. *In* Myelin Basic Protein. J. M. Boggs, editor. Nova Science, New York.
10. Bates, I. R., D. S. Libich, …, G. Harauz. 2002. An Arg/Lys→Gln mutant of recombinant murine myelin basic protein as a mimic of the deiminated form implicated in multiple sclerosis. *Protein Expr. Purif.* 25:330–341.
11. Bates, I. R., P. Matharu, …, G. Harauz. 2000. Characterization of a recombinant murine 18.5-kDa myelin basic protein. *Protein Expr. Purif.* 20:285–299.
12. Harauz, G., V. Ladizhansky, and J. M. Boggs. 2009. Structural polymorphism and multifunctionality of myelin basic protein. *Biochemistry.* 48:8094–8104.
13. Bates, I. R., J. M. Boggs, …, G. Harauz. 2003. Membrane-anchoring and charge effects in the interaction of myelin basic protein with lipid bilayers studied by site-directed spin labeling. *J. Biol. Chem.* 278:29041–29047.
14. Bates, I. R., J. B. Feix, …, G. Harauz. 2004. An immunodominant epitope of myelin basic protein is an amphipathic α-helix. *J. Biol. Chem.* 279:5757–5764.
15. Musse, A. A., J. M. Boggs, and G. Harauz. 2006. Deimination of membrane-bound myelin basic protein in multiple sclerosis exposes an immunodominant epitope. *Proc. Natl. Acad. Sci. USA.* 103: 4422–4427.
16. Musse, A. A., and G. Harauz. 2007. Molecular "negativity" may underlie multiple sclerosis: role of the myelin basic protein family in the pathogenesis of MS. *Int. Rev. Neurobiol.* 79:149–172.
17. Zhong, L., V. V. Bamm, …, V. Ladizhansky. 2007. Solid-state NMR spectroscopy of 18.5 kDa myelin basic protein reconstituted with lipid vesicles: spectroscopic characterization and spectral assignments of solvent-exposed protein fragments. *Biochim. Biophys. Acta.* 1768:3193–3205.
18. Chen, P. S., T. Y. Toribara, and H. Warner. 1956. Microdetermination of phosphorus. *Anal. Chem.* 28:1756–1758.
19. Fiske, C. H., and Y. Subbarow. 1925. The colorimetric determination of phosphorus. *J. Biol. Chem.* 66:375–400.
20. Smith, P. K., R. I. Krohn, …, D. C. Klenk. 1985. Measurement of protein using bicinchoninic acid. *Anal. Biochem.* 150:76–85.
21. Wiechelman, K. J., R. D. Braun, and J. D. Fitzpatrick. 1988. Investigation of the bicinchoninic acid protein assay: identification of the groups responsible for color formation. *Anal. Biochem.* 175:231–237.
22. Gor'kov, P. L., E. Y. Chekmenev, …, W. W. Brey. 2007. Using low-E resonators to reduce RF heating in biological samples for static solid-state NMR up to 900 MHz. *J. Magn. Reson.* 185:77–93.
23. Pines, A., M. G. Gibby, and J. S. Waugh. 1973. Proton-enhanced NMR of dilute spins in solids. *J. Chem. Phys.* 59:569–590.
24. Hohwy, M., C. M. Rienstra, and R. G. Griffin. 2002. Band-selective homonuclear dipolar recoupling in rotating solids. *J. Chem. Phys.* 117:4973–4987.
25. Hohwy, M., C. M. Rienstra, …, R. G. Griffin. 1999. Fivefold symmetric homonuclear dipolar recoupling in rotating solids: application to double quantum spectroscopy. *J. Chem. Phys.* 110:7983–7992.

26. Morris, G. A., and R. Freeman. 1979. Enhancement of nuclear magnetic resonance signals by polarization transfer. *J. Am. Chem. Soc.* 101:760–762.

27. Takegoshi, K., S. Nakamura, and T. Terao. 2001. C^{13}-H^{1} dipolar-assisted rotational resonance in magic-angle spinning NMR. *Chem. Phys. Lett.* 344:631–637.

28. Fung, B. M., A. K. Khitrin, and K. Ermolaev. 2000. An improved broadband decoupling sequence for liquid crystals and solids. *J. Magn. Reson.* 142:97–101.

29. Delaglio, F., S. Grzesiek, …, A. Bax. 1995. NMRPipe: a multidimensional spectral processing system based on UNIX pipes. *J. Biomol. NMR.* 6:277–293.

30. Morcombe, C. R., and K. W. Zilm. 2003. Chemical shift referencing in MAS solid state NMR. *J. Magn. Reson.* 162:479–486.

31. Markley, J. L., A. Bax, …, K. Wüthrich. 1998. Recommendations for the presentation of NMR structures of proteins and nucleic acids—IUPAC-IUBMB-IUPAB Inter-Union Task Group on the standardization of data bases of protein and nucleic acid structures determined by NMR spectroscopy. *Eur. J. Biochem.* 256:1–15.

32. Luca, S., D. V. Filippov, …, M. Baldus. 2001. Secondary chemical shifts in immobilized peptides and proteins: a qualitative basis for structure refinement under magic angle spinning. *J. Biomol. NMR.* 20:325–331.

33. Wishart, D. S., and B. D. Sykes. 1994. The ^{13}C chemical-shift index: a simple method for the identification of protein secondary structure using ^{13}C chemical-shift data. *J. Biomol. NMR.* 4:171–180.

34. Wang, Y. J., and O. Jardetzky. 2002. Probability-based protein secondary structure identification using combined NMR chemical-shift data. *Protein Sci.* 11:852–861.

35. Schwarzinger, S., G. J. Kroon, …, H. J. Dyson. 2001. Sequence-dependent correction of random coil NMR chemical shifts. *J. Am. Chem. Soc.* 123:2970–2978.

36. Libich, D. S., M. A. M. Ahmed, …, G. Harauz. 2010. Fuzzy complexes of myelin basic protein: NMR spectroscopic investigations of a polymorphic organizational linker of the central nervous system. *Biochem. Cell Biol.* 88:143–155.

37. Farès, C., D. S. Libich, and G. Harauz. 2006. Solution NMR structure of an immunodominant epitope of myelin basic protein. Conformational dependence on environment of an intrinsically unstructured protein. *FEBS J.* 273:601–614.

38. Boggs, J. M., M. A. Moscarello, and D. Papahadjopoulos. 1982. Structural organization of myelin: role of lipids-protein interactions determined in model systems. *In* Lipids-Protein Interactions. P. C. Jost and O. H. Griffith, editors. Wiley-Interscience, New York.

39. Filip, C., S. Hafner, …, H. W. Spiess. 1999. Solid-state nuclear magnetic resonance spectra of dipolar-coupled multi-spin systems under fast magic angle spinning. *J. Chem. Phys.* 110:423–440.

Biophysical Journal, Volume 99

Supporting Material

Solid-state NMR spectroscopy of membrane-associated myelin basic protein – conformation and dynamics of an immunodominant epitope

Mumdooh A.M. Ahmed, Vladimir V. Bamm, George Harauz, Vladimir Ladizhansky

Solid-state NMR spectroscopy of membrane-associated myelin basic protein – conformation and dynamics of an immunodominant epitope

Mumdooh A.M. Ahmed[1,3,4], Vladimir V. Bamm[2,3], George Harauz[2,3,$], Vladimir Ladizhansky[1,3,$].

Departments of [1]Physics, and [2]Molecular and Cellular Biology, and [3]Biophysics Interdepartmental Group, University of Guelph, 50 Stone Road East, Guelph, Ontario, N1G 2W1, Canada. [4]Current address: Department of Physics, Faculty of Science at Suez, Suez Canal University, Suez, Egypt.

SUPPORTING INFORMATION

Materials

Electrophoresis grade acrylamide, ultrapure TRIS base, and ultrapure Na_2EDTA were purchased from ICN Biomedicals (Costa Mesa, CA). Most other chemicals were reagent grade and acquired from either Fisher Scientific (Unionville, ON) or Sigma-Aldrich (Oakville, ON). The Ni^{2+}-NTA (nitrilotriacetic acid) agarose beads were purchased from Qiagen (Mississauga, ON). The lipids 1,2-dimyristoyl-*sn*-glycero-3-phosphocholine (DMPC), 1,2-dimyristoyl-*sn*-glycero-3-[phosphor-rac-(1-glycerol)] (sodium salt) (DMPG), and cholesterol (Chol) were purchased from Avanti Polar Lipids (Alabaster, AL). The phosphorus assay standard was purchased from Sigma-Aldrich (Oakville, ON). The BCA assay kit was purchased from Pierce (Rockford, IL). For uniform labeling and selective-labeling of protein for NMR spectroscopy, the stable isotopic compounds D_2O, $^{15}NH_4Cl$, $^{13}C_6$-glucose, and uniformly ^{13}C,^{15}N- labeled Asn and Val were obtained from Cambridge Isotope Laboratories (CIL, Andover, MA). For evaluation of reverse-labeling of protein, natural abundance Asn and Val were purchased from Sigma-Aldrich (Oakville, ON).

Evaluation of selective Val and Asn labeling in rmC1 and rmC8 variants.

The unmodified classic 18.5 kDa recombinant murine myelin basic protein (rmC1), and its quasi-deiminated variant (rmC8), were expressed in *E. coli* BL21-CodonPlus(DE3)-RP cells (Stratagene, La Jolla, CA) and purified as previously described [(1, 2)]. Uniformly ^{13}C,^{15}N-labeled protein was derived from cells grown in M9 minimal medium supplemented with $^{15}NH_4Cl$ and $^{13}C_6$-glucose [(3, 4)]. Selective-labeling of the Val and Asn residues in rmC1 and rmC8 was optimized as next.

In all preparations, both rmC1 and rmC8 concentrations were determined by measuring the absorbance at 280 nm, using ε=0.627 $Lg^{-1}cm^{-1}$ (as calculated by SwissProt for protein in 6.0 M guanidine hydrochloride, 0.02 M phosphate buffer, pH 6.5). Protein purity was routinely assayed by sodium dodecyl sulphate-polyacrylamide gel electrophoresis (SDS-PAGE). Following purification, all proteins were freeze-dried and stored at -20ºC prior to their use.

It was first necessary to test the selectivity of isotopic-labeling of valine and asparagine, and to optimize the level of added amino acids to M9 media during selective-labeling of protein, reverse-labeled protein was derived from cells grown in M9 medium supplemented with natural abundance Asn and Val at different molar concentrations ranging from 0.2 to 1 mM.

As the yield of rmC8 was always less than that of rmC1, more accurate measurement of the level of the degree of [Asn,Val]-isotopic labeling in each protein variant was performed using solution NMR. Three samples were investigated: the first sample was uniformly ^{13}C,^{15}N-labeled, whereas the other two were grown on M9 media supplemented with natural abundance NH_4Cl and glucose, and ^{13}C,^{15}N-labeled Val and Asn added at molar concentrations of 0.35 mM and 0.5 mM.

All samples examined by solution NMR were prepared by dissolving the freeze-dried protein in 500 µL of 30% (vol%) perdeuterated 2,2,2-trifluoroethanol (CF_3-C^2H_2-O^2H, TFE-d_2). Six samples were prepared from rmC1 and three from rmC8. **Table SI-1** shows the details of labeling of each sample.

Table SI-1. Composition of samples used for solution NMR spectroscopy.

Sample Name	Protein	Labeling	Concentration of added Asn and Val (mM)
S1	rmC1	U-^{13}C, ^{15}N	0
S2	rmC1	U-^{13}C, ^{15}N + NA-N, V[a]	0.2
S3	rmC1	U-^{13}C, ^{15}N + NA-N, V	0.35
S4	rmC1	U-^{13}C, ^{15}N + NA-N, V	0.5
S5	rmC1	U-^{13}C, ^{15}N + NA-N, V	0.75
S6	rmC1	U-^{13}C, ^{15}N + NA-N, V	1
S7	rmC8	U-^{13}C, ^{15}N	0
S8	rmC8	NA, U-^{13}C, ^{15}N-N, V	0.35
S9	rmC8	NA, U-^{13}C, ^{15}N-N, V	0.5

[a]N and V stands for asparagine and valine added to M9 media, respectively. Both N and V were natural abundance for rmC1 samples and U-^{13}C,^{15}N for rmC8 samples.

To characterize the degree of isotopic labeling and scrambling, we collected a series of standard ^{1}H-^{13}C and ^{1}H-^{15}N heteronuclear single quantum correlation (HSQC) spectra for rmC1 and rmC8 samples (s1-s9) dissolved in 30% TFE-d_2, and at room temperature. All experiments were performed on a Bruker Avance III spectrometer operating at a proton Larmor frequency of 600.13 MHz, using standard parameter sets [(5)]. All spectra were processed using NMRPipe. The peak assignments for rmC1 were published previously [(3, 4)]. Integration of peaks was done using SPARKY 3 (T. D. Goddard and D. G. Kneller, University of California, San Francisco), as well as using in-house written LUA script (www.lua.org) executed using the CARA (computer-aided resonance assignment) [(6)] built-in LUA interpreter.

We have collected ^{1}H-^{15}N and ^{1}H-^{13}C HSQC spectra on rmC1 (samples S1-S6), for which the spectroscopic assignments are known [(3, 4)]. The analysis of individual peak intensities corresponding to Val and Asn showed minimal transamination effects to Asn backbone and side chain ^{15}N, but some non-negligible transamination for Val.

The analysis of individual peaks or groups of peaks corresponding to different amino acid types in the ^{1}H-^{13}C HSQC spectra of samples S1-S6 revealed that for all amino acids but Asn, Val, and Leu, the HSQC peak intensities were comparable to their counterparts in the uniformly-labeled sample (S1), and that the degree of ^{13}C scrambling was generally low (albeit non-zero), and independent of the molarity of Asn and Val added to the M9 media (**Figure SI-1**). In other words, all the examined amino acid types but Asn, Val, and Leu, are mainly synthesized by the internal metabolic mechanisms of the *E. coli* cell strain used for over-expression of rmC1.

On the other hand, the Asn and Val cross peaks showed a dramatic reduction in their intensities. The degree of reverse-labeling was found to be relatively independent of the amount of added Asn and Val in the range 1 to 0.5 mM (**Figure SI-1**). In addition, leucine side chain signals were of relative intensities comparable to those of Asn and Val. This observation indicates that the Leu C^{β}, C^{γ} and $C^{\delta1/\delta2}$ are strongly scrambled because of the addition of Val to the growth media [(7, 8)].

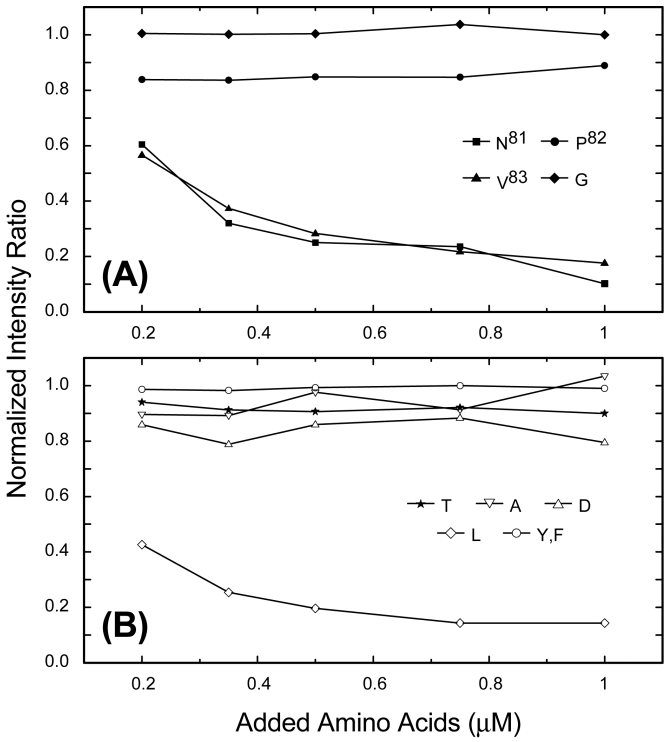

Figure SI-1. Normalized intensity ratios for selected peaks in the ^{1}H-^{13}C HSQC (heteronuclear single quantum coherence) spectrum of rmC1: (A) H^{α}-C^{α}, and (B) H^{β}-C^{β}. The intensity/sum-over-box ratios of each spectrum at a given added amount of amino acids was first normalized by dividing the ratios by the median of intensity ratios of the central 75% of the population in each spectrum. The selected peaks are plotted here as a function of the molarity of the added amino acids in M9 medium during recombinant murine MBP (rmC1 or rmC8) over-expression.

Similar experiments were performed on the quasi-deiminated variant rmC8, and showed reduced levels of over-expression compared to rmC1, which is why a more precise test of the level of scrambling was performed. Because the spectroscopic assignments of rmC8 are as yet unknown, a [U-^{13}C, ^{15}N]-labeled rmC8 (S7) and two [U-^{13}C, ^{15}N-Val, Asn]-labeled samples (S8 and S9, **Table SI-1**) were prepared, and the peak intensities were compared. The level of valine and asparagine labeling was estimated to be ~33-40% when 0.35 mM of the amino acids were added, and increased to 66-75% for 0.5 mM of added amino acids. The Leu C^{β}, C^{γ} and $C^{\delta 1/\delta 2}$ correlations were found to be of comparable intensities to Val, whereas most other residues were labeled in the range of 2-13%.

In summary, supplementing the media with the appropriate concentration of isotopically-labeled valines and asparagines resulted in the incorporation of labeled amino acids into the over-expressed protein at relatively high levels. Most other amino acids were synthesized from the internal metabolic mechanisms of the *E. coli* strain that we used. The only noticeable exception was leucine, in which the C^{β}, C^{γ}, and C^{δ} carbons were synthesized from Val C^{α}, C^{β}, and C^{γ} [(8)].

Solid-state NMR spectroscopy

Table SI-2. Acquisition parameters for two-dimensional spectra[a].

Spectrum-Sample	Temperature (°C)	t_1- points	Number of scans
(CO)N(CO)CA	-25	60	1792
^{13}C-^{13}C-rmC1[b]	-25	512	152
^{13}C-^{13}C-rmC1[c]	10	320	200
^{13}C-^{13}C-rmC1[c]	20	320	160
^{13}C-^{13}C-rmC8[b]	-25	512	128
^{13}C-^{13}C-rmC8[d]	10	320	256
^{13}C-^{13}C-rmC8[d]	20	320	256
^{1}H-^{13}C INEPT-HETCOR[e]	35	128	192
^{1}H-^{13}C CP-HETCOR[e]	35	128	384

[a]All spectra were acquired on a 600 MHz spectrometer with a 12 kHz MAS rate, except for the ^{1}H-^{13}C correlations of rmC1 which were acquired on a 800 MHz spectrometer with a 14.3 kHz MAS rate.
[b]DARR (dipolar assisted rotational resonance) mixing of 10 and 20 ms for rmC1 and rmC8, respectively.
[c]Spin-diffusion mixing of 150 ms.
[d]DARR mixing of 150 ms.
[e]The same acquisition parameters were used for rmC1 and rmC8.

Table SI-3. Chemical shift assignments at -25°C for membrane-associated rmC1 and rmC8.

Nucleus	MBP isoform	
	rmC1	rmC8
Asn81- C^{α}	52.1	52.4
Asn81- C^{β}	39.9	40.1
Val83- C^{α}	66.3	66.3
Val83- C^{β}	31.3	31.4
Val84- C^{α}	67.0	66.8
Val84- C^{β}	31.9	31.8
Asn89- C^{α}	52.9	53.5
Asn89- C^{β}	40.3	40.4
Val91- C^{α}	62.3	62.3
Val91- C^{β}	32.1	32.3

REFERENCES for SUPPORTING INFORMATION

1. Bates, I. R., D. S. Libich, D. D. Wood, M. A. Moscarello, and G. Harauz. 2002. An Arg/Lys -> Gln mutant of recombinant murine myelin basic protein as a mimic of the deiminated form implicated in multiple sclerosis. *Prot Express Purif* 25:330-341.
2. Bates, I. R., P. Matharu, N. Ishiyama, D. Rochon, D. D. Wood, E. Polverini, M. A. Moscarello, N. J. Viner, and G. Harauz. 2000. Characterization of a recombinant murine 18.5-kDa myelin basic protein. *Prot Express Purif* 20:285-299.
3. Libich, D. S., M. M. Monette, V. J. Robertson, and G. Harauz. 2007. NMR assignment of an intrinsically disordered protein under physiological conditions: the 18.5 kDa isoform of murine myelin basic protein. *Biomol NMR Assign* 1:61.
4. Libich, D. S., V. J. Robertson, M. M. Monette, and G. Harauz. 2004. Backbone resonance assignments of the 18.5 kDa isoform of murine myelin basic protein (MBP). *J Biomol NMR* 29:545-546.
5. Braun, S., H.-O. Kalinowski, and S. Berger. 1998. 150 and More Basic NMR Experiments: A Practical Course. Wiley-VCH, Weinheim.
6. Keller, R. 2004. The computer aided resonance assignment tutorial. Cantina Verlag, Goldau, Switzerland.
7. Monticello, D. J., and R. N. Costilow. 1982. Interconversion of valine and leucine by Clostridium sporogenes. *J Bacteriol* 152:946-949.
8. Sylvester, S. R., S. Y. Lan, and C. M. Stevens. 1981. In vitro conversion of leucine to valine: configurational assignment of [5-13C]leucines. *Biochemistry* 20:5609-5611.